HAL open science

Local Effects of Organic Inhibitor Molecules on Passivation of Grain Boundaries Studied In Situ on Copper

Sagar B Sharma, Vincent Maurice, Lorena H Klein, Philippe Marcus

▶ **To cite this version:**

Sagar B Sharma, Vincent Maurice, Lorena H Klein, Philippe Marcus. Local Effects of Organic Inhibitor Molecules on Passivation of Grain Boundaries Studied In Situ on Copper. Journal of The Electrochemical Society, 2021, 168 (6), pp.061501. 10.1149/1945-7111/ac0308 . hal-03252979

HAL Id: hal-03252979

https://hal.science/hal-03252979v1

Submitted on 8 Jun 2021

HAL is a multi-disciplinary open access archive for the deposit and dissemination of scientific research documents, whether they are published or not. The documents may come from teaching and research institutions in France or abroad, or from public or private research centers.

L'archive ouverte pluridisciplinaire **HAL**, est destinée au dépôt et à la diffusion de documents scientifiques de niveau recherche, publiés ou non, émanant des établissements d'enseignement et de recherche français ou étrangers, des laboratoires publics ou privés.

Journal of The Electrochemical Society, 2021 **168** 061501

Local Effects of Organic Inhibitor Molecules on Passivation of Grain Boundaries Studied In Situ on Copper

Sagar B. Sharma, Vincent Maurice,[z] Lorena H. Klein, and Philippe Marcus[*,z]

[1]*PSL University, CNRS-Chimie ParisTech, Institut de Recherche de Chimie Paris (IRCP), Physical Chemistry of Surfaces Group, 75005 Paris, France*

The effects of two organic corrosion inhibitors, 2-mercaptobenzothiazole (MBT) and 2-mercaptobenzimidazole (MBI), on grain boundary passivation was investigated on copper at the nanometer scale in NaOH solution using electrochemical scanning tunneling microscopy (ECSTM). Global electrochemical analysis by cyclic voltammetry showed that the organic surface layers, pre-formed after reductive dissociation of the native oxide in the presence of the inhibitors, block the formation of a Cu(I) surface oxide and thus passivation, but do not entirely suppress residual reactivity. Local ECSTM analysis in initial metallic, subsequently oxidized, and final reduced states confirmed residual intergranular reactivity except for coherent twins. On coincidence site lattice (CSL) and random boundaries, residual dissolution with accumulation of corrosion products or residual passivation was observed, depending on the barrier effect of the pre-formed inhibitor layer on oxide formation. For low Σ CSLs, no difference of barrier effect was observed between MBT and MBI. For more reactive high Σ CSLs and random boundaries, pre-adsorbed MBT formed a stronger barrier against passivation by oxide growth than pre-adsorbed MBI. The results provide deeper understanding of how passivation is altered by a pre-formed surface layer of organic corrosion inhibitor, including locally at different grain boundary types.

© 2021 The Author(s). Published on behalf of The Electrochemical Society by IOP Publishing Limited. This is an open access article distributed under the terms of the Creative Commons Attribution 4.0 License (CC BY, http://creativecommons.org/licenses/by/4.0/), which permits unrestricted reuse of the work in any medium, provided the original work is properly cited. [DOI: 10.1149/1945-7111/ac0308]

Manuscript submitted April 7, 2021; revised manuscript received May 6, 2021. Published June 4, 2021.

Supplementary material for this article is available online

Grain boundaries (GBs) play a crucial role for the durability of polycrystalline metallic materials. Their surface terminations are the sites of initiation of intergranular corrosion, which, if not mitigated by corrosion inhibitors or by formation of a passivating surface oxide, propagates into the sub-surface region and eventually leads to failure of the entire microstructure.

From grain boundary engineering studies, it is established that, among the two main classes of GBs, only high angle GBs, characterized by a misorientation angle larger than 15°, are susceptible to intergranular corrosion because of their higher energy than low angle GBs.[1–20] High-angle GBs can be sub-divided into two classes: (i) coincidence site lattices (CSL) boundaries denoted by a Σn index, where 1 n^{-1} refers to the fraction of lattice sites shared by the two crystals at the interface, and (ii) random boundaries for which the value of n exceeds[21] Some CSL boundaries are also called "special boundaries" when they have comparatively lower reactivity, owing to their lower boundary energy, than random or other CSL boundaries. Coherent twins (CTs), which are CSL Σ3 boundaries having a GB plane of {111} orientation, are most common in *fcc* materials such as copper and have better resistance to corrosion than any other CSLs.

Early-stage intergranular dissolution of copper in the active state and transient dissolution during passivation have been studied in situ at the nanometric scale using electrochemical scanning tunneling microscopy (ECSTM).[22–26] Surface GB terminations assigned to coherent twins showed weaker dissolution, both in active and passive states, than GB edges assigned to other CSL or random boundaries. Combining ECSTM with electron back-scatter diffraction (EBSD) characterization of the same local GB sites, the passivation behavior of coherent twins was found to depend on the deviation angle of the GB plane from its perfect {111} orientation with a transition from more to less efficient passivation for a deviation angle of 0.4°–0.5°[26] For random boundaries, passivation in the Cu(I) oxidation range was characterized by a decrease of the depth of GB edge region due to the formation of a passive film locally thicker than on the adjacent grains, and thus to anodic oxidation being locally less efficient since consuming more copper at the grain boundaries[26]

A practical approach to mitigate and control metals and alloys corrosion in aggressive environments is by using corrosion inhibitors. Organic molecules such as azole derivatives are frequently used as corrosion inhibitors for copper and its alloys.[21,27–35] Two such molecules are 2-mercaptobenzothiazole (MBT, $C_7H_5NS_2$) and 2-mercaptobenzoimidazole (MBI, $C_7H_6N_2S$), which have shown to be very efficient inhibitors for copper systems.[36–54] Being classified as mixed-type inhibitors mitigating both the anodic and cathodic activity,[27,42,47,51–53] MBT and MBI have been reported as efficient inhibitors in neutral, acidic, or alkaline conditions.[27,29,36–41,43,45,46,50–52] What makes MBT and MBI very efficient inhibitors is that they include sulfur and nitrogen atoms within their heterocyclic structure, two S and one N atom in MBT and one S and two N atoms in MBI. These atoms can, simultaneously or individually, strongly bond to the copper atoms of the surface, either in metallic or oxidized state. Thus a stable molecular film forming a barrier that protects the copper surface from its environment is stabilized by chemisorption.[29,34,36,39,40,43,45,48,50,52,55–64]

For MBT, a Cu-MBT surface film would form with thickness depending on the pH of the medium,[36,37] ranging from only a monolayer film in conditions where a stable Cu_2O oxide is formed (pH > 4) to the formation of multilayers in acidic conditions where no stable Cu_2O film can be formed (pH < 3).[48,52] The proposed formation mechanism is one where surface ions of Cu(I) react to adsorbed MBT.[34,42] However, if MBT pre-adsorption occurs on the copper in the metallic state, in that case, the MBT monolayer prevents the formation of a surface oxide as observed in alkaline conditions[30,33] or gaseous phase[55–57,59] For MBI, several studies have proposed the formation of a polymeric film,[36,39,43,46,47] with Cu reaction products included in the film and depending on the initial surface state of copper, metallic or oxidized, before the formation of the protective film[39] Cu-MBI[39] or Cu_2-MBI[36] organometallic complexes have been suggested. MBI also blocks surface oxidation as observed in the gas phase.[63,64]

The local effects of these two organic corrosion inhibitors on the dissolution of copper in the active state at the surface termination of different types of grain boundaries were recently studied in situ in acid solution by ECSTM.[65,66] Global electrochemical analysis

*Electrochemical Society Fellow.
[z]E-mail: vincent.maurice@chimieparistech.psl.eu; philippe.marcus@chimieparistech.psl.eu

confirmed efficient corrosion inhibition by a MBT surface layer, pre-adsorbed before the corrosion test and protecting the grains by blocking Cu(I) anodic dissolution. Local analysis showed that while the pre-formed MBT layer perfectly protects the low ∑ CSL GBs, the more reactive random GBs are subject to local accumulation of reaction products resulting from preferential intergranular dissolution. MBI inhibition was less efficient than MBT inhibition. Cu(I) reaction products were generated on the grains to form a protective surface film, and their preferential local accumulation was observed more frequently in the analyzed population of intergranular sites than with MBT.

Here, we report the in situ nanometric characterization of the effects of organic layers of MBT and MBI, pre-formed on the metallic surface, on the local passivation properties of copper at GB surface terminations. The study was conducted in alkaline NaOH (aq) aqueous solutions in the potential range of Cu(I) anodic oxidation where, in the absence of inhibitor, a stable Cu_2O passive film is formed[23,24,26,67–80] Local ECSTM in situ analysis at the nanometer scale was combined with global electrochemical analysis performed by cyclic voltammetry (CV). Although MBT and MBI are well established as corrosion inhibitors for polycrystalline copper, copper alloys and other materials, and further substantiated by our work on early-stage intergranular corrosion in acid solution,[65,66] there are no studies, to the best of our knowledge, that have addressed the impact of MBT and MBI on copper passivation at grain boundaries terminations. This work brings new insight on alterations of copper passivation properties brought by pre-adsorbed organic inhibitor molecular films and on local effects at surface terminations of different types of GBs.

2. Experimental

The experiments were performed with microcrystalline samples obtained by cryogenic rolling after freezing in liquid nitrogen of high-purity cast electrolytic tough pitch copper.[22–26,65,66,81–83] In order to ensure the relatively smaller grain size necessary for the microstructure to be included in the STM field of view, the annealing treatment for full recrystallization of the samples was limited in time and temperature of 1 min and 200 °C, respectively. The resulting samples showed no preferential grain orientation, i.e. nearly random texture, as confirmed by EBSD.[8–83] 66% of GB length corresponded to ∑3 CSL boundaries, while the remaining 34% were, for the most part, random boundaries. The surface preparation was done following the protocol previously reported[84] starting with mechanical polishing with diamond spray from 6 μm down to 0.25 μm which was followed by electrochemical polishing in 66% orthophosphoric acid for 15 s at 3 V versus a copper counter electrode to remove the cold work layer.

The ECSTM analysis was carried using an Agilent Technologies system ((PicoSPM base, Keysight STM S scanner, PicoScan 2100 controller, PicoStat bi-potentiostat and Picoscan software). The ECSTM cell, homemade from Kel-f, can contain ~350 μl of electrolyte. The working electrode area was delimited to 0.16 cm^2 by using a VITON® O-ring. The counter electrode and the pseudo reference electrode (+0.20 V/SHE) were made from two 0.5 mm diameter Pt wires. The ECSTM cell, with counter and reference electrodes pre-mounted, was cleaned using the previously established procedure and tips were prepared using an electrochemical etching of a 0.25 mm diameter tungsten wire and were covered with Apiezon wax except at the apex.[84]

A non-deaerated 0.1 M NaOH(aq) electrolyte solution (pH 13) was prepared from ultrapure NaOH (Sigma-Aldrich) and Millipore water (resistivity > 18 MΩ cm). Solutions of MBT and MBI in the concentration of 1 mM were prepared by dissolution in the electrolyte from 99% and 98% pure powders, respectively (Sigma-Aldrich). The sample was exposed to the electrolyte to the open circuit potential (E_{OCP} = −0.03 V/SHE). The air-formed surface oxide was reduced by cathodic reduction of the sample (scanning at 20 mV s^{-1}) down to E = −1.20 V/SHE at the onset of hydrogen evolution and upward to E = −0.75 V/SHE, remaining in the Cu(0) potential range. Three such cycles were applied to reduce the native oxide fully. The ECSTM images of the microcrystalline copper surface were first taken in the Cu(0) metallic state at E = −0.75 V/SHE in a local area rich in different types of grain boundaries. Surface imaging in the metallic state was followed by imaging the surface in the Cu(I) oxidation range. This was done by polarizing the sample anodically up until E = −0.08 V/SHE at the scan rate of 1 mV s^{-1}. The tip was always kept engaged (but not scanning) during the potential scan so as to not lose the previously observed area of interest. The surface was imaged again in the Cu(I) oxidation range at E = −0.08 V/SHE. Following this, the surface was imaged again in the reduced state. This is done by sweeping the sample's potential down to E = −1.20 V/SHE, followed by upward to E = −0.75 V/SHE at 1 mV s^{-1}. Again the tip was kept engaged but not scanning. Images of the surface in the initial metallic, subsequently oxidized and final reduced states were recorded in constant current mode without the usage of any filters. The recorded images were processed with Gwyddion software.[85]

The topography across the GB regions was measured by line profile analysis. For analysis, a GB site was selected and 30 adjacent line scans covering a local distance of ~170 nm along the boundary were drawn across the grain boundary. The GB depth was taken as to be the local difference in topographic height between the bottom of the GB regions and the surface level of the corresponding grains on either side of the GB. Each such selected site was subject to ten different measurements and the standard deviations of these ten measurements are reported in the form of an error bar.

Results and Discussion

Macroscopic MBT and MBI effects on passivation.—Before discussing the ECSTM data, it is important to understand the global electrochemical behavior of the surface. For this, cyclic voltammetry was applied using the same protocol as for the ECSTM study in order to understand the effect of the presence of MBT and MBI in the NaOH alkaline electrolyte on passivation at the macroscopic scale. The CVs were obtained in the ECSTM cell after the cathodic reduction of the native oxide and recorded starting from −0.75 V/SHE up to the anodic apex of −0.08 V/SHE, in the domain of Cu(I) anodic oxidation, then down to the cathodic apex of −1.2 V/SHE, at the beginning of the hydrogen evolution region, and back to the starting point. The recorded macroscopic electrochemical response can be assigned to the properties of the grains since, for the total exposed surface, the surface fraction of the grains is much larger than that of the GBs.

Figure 1 shows the superimposed CVs of microcrystalline copper obtained in 0.1 M NaOH(aq), in 0.1 M NaOH(aq) + 1 mM MBT, and in 0.1 M NaOH(aq) + 1 mM MBI. The analysis of the anodic

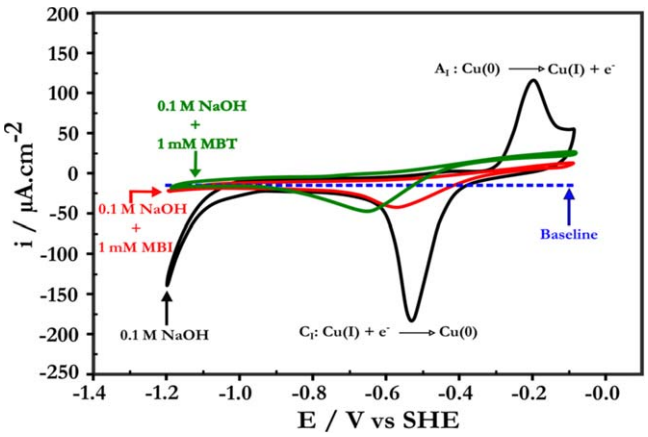

Figure 1. Cyclic voltammograms in the ECTM cell for microcrystalline copper in 0.1 M NaOH(aq) with and without MBT and MBI as indicated, scan rate = 1 mV s^{-1}.

and cathodic reactions for all three cases is made according to the drawn baseline. The baseline was drawn for 0.1 M NaOH(aq) so that it is well centered in the potential region of −0.9 to −0.7 V/SHE, where the measured current is minimum. The same procedure was used for the two cases with inhibitors, and the current offsets were adjusted so that the baselines superimpose with that in the pure electrolyte.

In pure 0.1 M NaOH(aq), during the anodic scan, a shallow anodic peak is observed at −0.42 V/SHE followed by a sharp and intense A_I peak at −0.2 V/SHE. The latter is characteristic of the anodic oxidation of copper as labeled in Fig. 1,[67–80] and the former is likely related to the adsorption of hydroxide groups in the underpotential range of oxidation, as studied on single crystals.[76–79] During the cathodic scan and with respect to the baseline, the reaction remains anodic until −0.38 V/SHE and is cathodic afterwards. A sharp C_I cathodic peak is observed at −0.52 V/SHE corresponding to the reductive decomposition of the Cu(I) oxide to Cu(0) metal as labeled in Fig. 1, after which the cathodic current decreases to a stable plateau till the onset of hydrogen evolution. The measurements are in good agreement with those from previous work in the same electrolyte.[24,26,67,68,77–79]

In 0.1 M NaOH(aq) + 1 mM MBT, during the anodic scan, the CV does not show any A_I anodic peak of formation of the Cu(I) passive oxide film, but instead a continuous although attenuated increase of positive current from about −0.75 V/SHE up until the anodic apex at −0.08 V/SHE. During the cathodic scan, the current remains anodic down till −0.51 V/SHE, after which it is cathodic with a small peak observed at −0.62 V/SHE. The C_I peak observed in pure 0.1 M NaOH(aq) at −0.52 V/SHE, and characteristic for the reduction of the Cu(I) passive oxide film to Cu(0) metal, is suppressed. These measurements confirm the inhibiting effect of the presence of a pre-formed layer of MBT on a reduced copper surface on the formation of the Cu(I) surface oxide, like previously observed in alkaline aqueous solution[30,33] and in gaseous phase.[56,57,59]

In the presence of 1 mM MBI in the 0.1 M NaOH(aq) electrolyte, no A_I anodic peak is observed on polarizing the sample anodically and the C_I reduction peak is also suppressed in the cathodic scan. Thus, the pre-formed layer of MBI also inhibits the formation of the Cu(I) surface oxide, like observed after exposure to gaseous oxygen.[63,64] The measured currents are lower than in the presence of MBT with an increase of positive current from about −0.60 V/SHE and slow and continuous till the anodic apex. During the cathodic scan, the current remains anodic down till −0.40 V/SHE, after which it is cathodic with a small peak observed at −0.54 V/SHE. Note that, with both MBT and MBI, the negative current measured at the cathodic apex is strongly decreased, showing that the pre-formed organic layers also inhibit the cathodic activity in the potential range of hydrogen evolution.

Unlike in strongly and weakly acidic conditions (pH < 5), Cu exibits passivity in the alkaline conditions of the present experiment (pH = 13). This means that, in the absence of the inhibitors, when the surface is swept anodically, a stable Cu_2O oxide is formed in the Cu(I) oxidation range that protects the surface against dissolution. The cathodic peak C_I observed in pure 0.1 M NaOH(aq) confirms the formation of the surface oxide and corresponds to the decomposition of this Cu(I) oxide to Cu(0) metallic copper.[67–80] It is important to keep in mind that in 0.1 M NaOH(aq), during anodic passivation, there is a competing reaction occurring between the dissolution of copper into the electrolyte and the formation of the stable oxide. Both reactions consume metallic copper but the first one is minority and irreversible whereas the second one is largely dominant and reversible.

On integrating the measured current densities over time, we obtain charge densities for the anodic and cathodic reactions as $q_{AI} = 2.357 \times 10^{-3}$ C.cm^{-2} and $q_{CI} = 2.168 \times 10^{-3}$ C.cm^{-2}, respectively, confirming a partially reversible behavior consistent with some copper being irreversibly consumed during anodic polarization since $q_{AI} > q_{CI}$. The electric charge density q associated with the irreversible reaction of copper is 1.89×10^{-4} C.cm^{-2} ($q = q_{AI} - q_{CI}$). The equivalent thickness of irreversibly dissolved copper ($\delta_{Cu(IR)}$) can be calculated using Eq. 1, where V_M is the molar volume of reacting material ($V_M^{Cu} = 7.1$ cm^{3}mol^{-1} for Cu metal), z the number of exchanged electrons (z = 1 for Cu(I) anodic oxidation) and F the Faraday constant.

$$\delta = \frac{qV_M}{z} \quad [1]$$

From this, we get a $\delta_{Cu(IR)}$ value of 0.14 nm. This low value amounts to 0.67 equivalent monolayers (ML) of copper being irreversibly consumed by dissolution. Indeed, one {111}-oriented ML of copper is 0.208 nm thick from the bulk *fcc* structure of copper. To calculate the equivalent thickness of the Cu(I) passive oxide film formed on the surface, we use the value q_{CI} of the reductive electric charge density in Eq. 1. If one assumes the formation of $Cu(I)_2O$ oxide and using $V_M^{cu_2o} = 23.9$ cm^3.mol^{-1} and z = 2 for the reduction of 2 Cu(I) in Eq. 1, we obtain the value of $\delta_{pass} = 2.68$ nm. This obtained value is in agreement with the previously obtained thickness values for Cu(I) oxide films.[24,26,67–79]

Regarding the effect of MBT and MBI, we have seen in Fig. 1 that the distinct anodic peak A_I is absent when the CV is recorded in the presence of the inhibitor. This implies that the pre-formed MBT and MBI layers block passivation of the surface by inhibiting the formation of the surface oxide. The residual activity measured both during the anodic and cathodic scans in the presence of inhibitor may be due to the oxidation and reduction of those copper atoms that are dissociated from oxygen during the initial cathodic reduction pretreatment of the air-formed native oxide. Indeed, the cathodic pretreatment is applied in the presence of the inhibitors and it is most likely that the free Cu atoms, dissociated from oxygen by electrochemical reduction, are unstable, react with the adsorbed organic molecules and are thus captured in the molecular inhibitor layer formed on the surface. So, we can expect the inhibitor film, pre-formed before the CV treatment, to include copper atoms originating from the native oxide and trapped in the organic film as illustrated by the model shown in Fig. 2. The residual activity recorded during anodic and subsequent cathodic polarization of the surface can thus be that of the Cu atoms initially trapped in the pre-formed inhibitor surface layer.

Since surface oxide formation is blocked by the inhibitor layer pre-formed before electrochemical testing, the equivalent thickness δ_{pass} of the Cu(I) passive oxide film is not calculated since it is not physically meaningful. Instead, the value $\delta_{Cu(R)}$, calculated from the cathodic charge density, is assigned to the amount of copper that is reversibly reacting during the electrochemical polarization. This value estimates the amount of copper presumably trapped in the pre-formed inhibitor layer and reversibly reacting during the CV treatment. The other quantity, $\delta_{Cu(IR)}$, calculated from the difference between anodic and cathodic charge density, estimates the amount of copper that is irreversibly consumed due to the residual dissolution occurring during the electrochemical polarization.

With MBT, the values of the charge density cumulated during the anodic and cathodic polarization scans are 1.807×10^{-3} C.cm^{-2} and 1.746×10^{-3} C.cm^{-2}, respectively. From the cumulated cathodic charge density, we get $\delta_{Cu(R)} = 1.28$ nm (6.17 Ml) of copper trapped in the pre-formed inhibitor film and reversibly reacting during electrochemical polarization, meaning that several equivalent monolayers of copper would be trapped in the pre-formed MBT surface layer as a result from the dissociation of the native oxide. The non-zero difference between the anodic and cathodic charge densities is consistent with an irreversible loss of copper due to residual dissolution. From the difference of 6.1×10^{-5} C.cm^{-2}, $\delta_{Cu(IR)}$ is calculated from Eq. 1 using $V_M^{Cu} = 7.1$ cm^{3}mol^{-1} and z = 1, and we get $\delta_{Cu(IR)} = 0.045$ nm corresponding to a fraction of a monolayer (0.22 Ml) of copper irreversibly consumed due to residual dissolution. This quite small value is consistent with efficient macroscopic

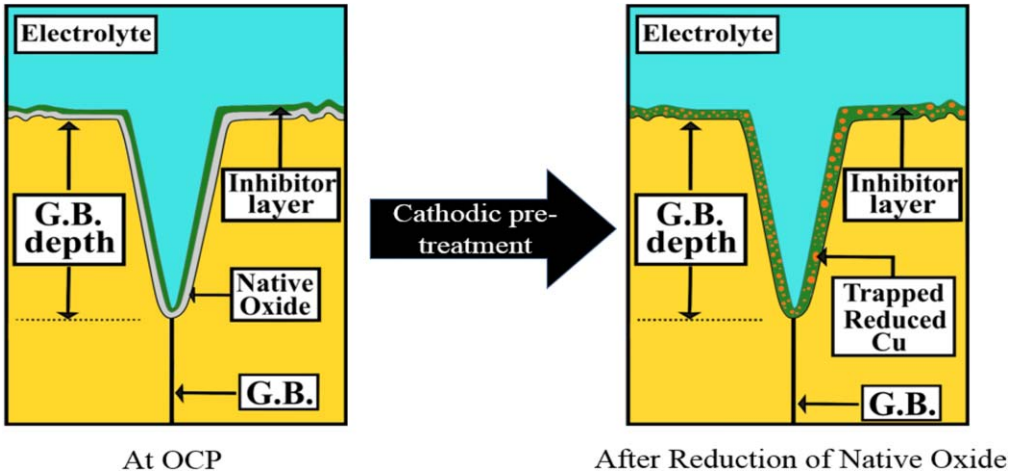

Figure 2. Schematic illustration of the inhibitor layer formed after cathodic pre-treatment of the surface: the reduction of the native oxide pre-covered by the inhibitor film leads to trapping of the copper atoms dissociated from the oxygen atoms in the organic inhibitor layer.

inhibition of irreversible dissolution and residual dissolution being localized in the most active sites such as grain boundary surface terminations. With MBI, the values of the anodic and cathodic charge densities are 8.47×10^{-4} C.cm^{-2} and 8.42×10^{-4} C.cm^{-2}, respectively. For $\delta_{Cu(R)}$, we get a value of 0.62 nm (2.98 Ml) from the cathodic charge density, meaning that the pre-formed MBI inhibitor layer would contain about twice as less reacting copper atoms than the pre-formed MBT inhibitor layer. The difference between anodic and cathodic charge densities is within the uncertainty range, which suggests that the pre-formed MBI inhibitor layer would more efficiently mitigate irreversible dissolution than the pre-formed MBT inhibitor layer in the most reactive surface sites.

In summary, these CV data show that the organic inhibitor layers, pre-formed before electrochemical testing, behave similarly and block the formation of a Cu(I) oxide film and thus surface passivation. However, the electrochemical reactivity is not fully suppressed. The observed residual activity is assigned for its most part to the copper atoms dissociated from the native oxide during the cathodic pretreatment and trapped in the pre-formed inhibitor surface layer. These trapped copper atoms amount to the equivalent of a few monolayers of copper metal and react reversibly upon anodic and cathodic polarization. Irreversible anodic charge transfer is assigned to the residual anodic dissolution of copper contributed preferentially from the most reactive sites of the surface such as GB surface terminations. Although blocking passivation may seem detrimental to corrosion protection, this is efficiently compensated by the barrier property of the pre-formed organic layers efficiently mitigating dissolution upon anodic polarization in the Cu(I) oxidation range.

ECSTM images and classification of grain boundaries by their morphology.—Figures 3a and 3b show in situ ECSTM images of the topmost surface of microcrystalline copper obtained in the presence of MBT or MBI in the 0.1 M NaOH(aq) electrolyte, respectively. For each inhibitor, the same local microstructure could be imaged in the initial metallic state, after reduction of the native oxide (Figure S1a in Supplementary Information (available online at stacks.iop.org/JES/168/061501/mmedia)), in the Cu(I) oxidation range (Figure S1b in Supplementary Information) and in the final metallic state, after reduction of the oxidized state (Figure S1c in Supplementary Information). The selected areas of interest show the typical copper microstructure exhibiting grains and sub-grains. The difference in measured topographic height amongst different grains is attributed to differences of local surface reactivity during the surface preparation by electrochemical polishing. The GB surface regions correspond to the surface termination of the GB planes and their adjacent vicinity. Some of these GB surface regions are measured higher than others, which is again assigned to differences in local surface reactivity during the surface preparation.

The adopted classification of the observed grain boundaries is based on their morphology in the surface plane and is consistent with our previous work.[65,66] GBs appearing in parallel pairs and separating sub-grains are assigned to Σ3 coherent twins, i.e. with a GB plane of {111} orientation. Short and straight GBs are assigned to low Σ CSL boundaries (including other Σ3 CSLs than coherent twins). Straight segments observed along a GB with locally straight or curved morphology are assigned to high Σ CSL boundaries. Finally, curved GBs or locally curved segments are assigned to random boundaries. A summary of grounds used for this classification is given in Table I.

Local MBT and MBI effects on passivation of grain boundary network.—The analysis of the two series of images displayed in Figure S1 resulted in two populations of local GB sites where the depth of the GB surface regions could be measured geometrically in the initial Cu(0) metallic state of the surface, in the oxidized state upon anodic polarization in the Cu(I) potential region, and back in the Cu(0) metallic state following reduction of the oxidized state. These two populations of 101 GB sites for MBT and 100 GB sites for MBI are indexed in Fig. 3 and color-coded according to the locally observed GB behavior. Indeed, for both inhibitors, comparative analysis of the variations of the measured depth of all GB sites resulted in five distinct types of local topographical evolution of the grain boundary network that are: (i) no variation of the GB depth

Table I. Summary of criteria used for classification of grain boundaries based on their morphology in the surface plane.

GB morphology	Class of GBs
Two parallel GBs separating a sub-grain	Σ 3 coherent twins (with a {111}-oriented GB plane)
Short and straight GBs	Low Σ CSL boundaries
Straight GB segments	High Σ CSL boundaries
Curved GBs or curved GB segments	Random boundaries

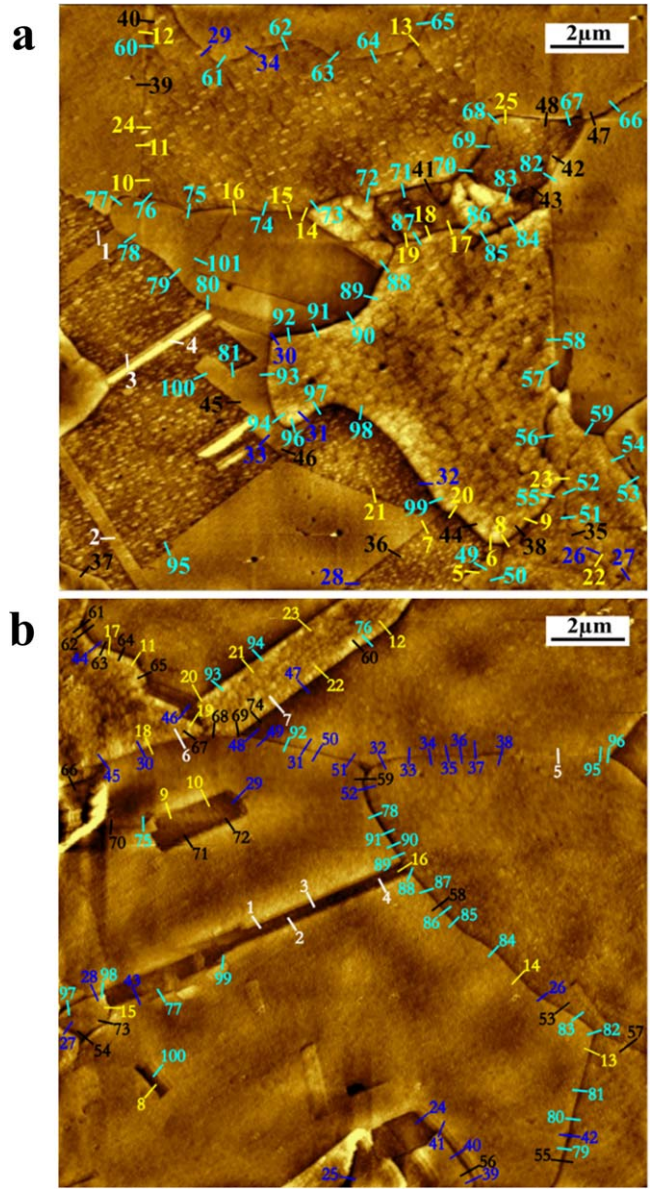

Figure 3. Topographic ECSTM images of microcrystalline copper obtained in 0.1 M NaOH(aq) with (a) MBT or (b) MBI: (a) $\Delta Z = 10.2$ nm, $E_{Cu} = -0.75$ V/SHE, $E_{tip} = -0.30$ V/SHE, $I_t = 0.5$ nA; (b) $\Delta Z = 9.8$ nm, $E_{Cu} = -0.75$ V/SHE, $E_{tip} = -0.60$ V/SHE, $I_t = 0.5$ nA GB sites are color-coded according to their behavior: (white) no depth variation in metallic, oxidized and reduced surface states; (yellow) continuous depth increase; (dark blue) continuous depth decrease; (black) depth decrease and subsequent increase; (light blue) depth increase and subsequent decrease.

(sites indexed in white in Fig. 3), (ii) repeated increase of the GB depth (sites indexed in yellow in Fig. 3), (iii) repeated decrease of the GB depth (sites indexed in dark blue in Fig. 3), (iv) decrease followed by an increase of the GB depth (sites indexed in black in Fig. 3), and (v) increase followed by a decrease of the GB depth (sites indexed in light blue in Fig. 3). For each type of local GB behavior, one example of the line profile evolution is presented in Fig. 4 for the GB sites indexed in Fig. 3a.

These five types of local topographical evolution are similar to those observed when studying the early intergranular corrosion in acidic conditions (10 mM HCl, pH 2) in the presence of the inhibitors.[65,66] However, their mechanistic interpretations differ as one must take into account the inhibitor effect on surface oxidation and formation of the passive film. These five types of GB local behavior show that both inhibitors block surface oxide formation and thus passivation in the GB regions in agreement with the global CV data, but that residual intergranular reactivity of dissolution or oxide formation, i.e. passivation, is not suppressed in the GB regions. Hereafter, we organize the discussion according to the type of GB behavior locally observed.

Intergranular passivation blocked with no residual preferential reactivity at GBs.—The local GB sites that show no variation of the GB depth upon anodic oxidation and subsequent reduction are labeled 1 to 4 in Figs. 3a and 3b. The depth values measured across these GB sites are reported in Figure S2a and b in Supplementary Information for MBT and MBI, respectively. In these local sites, the absence of depth variation indicates no preferential reactivity of the GB surface regions as compared to the adjacent grains. This behavior is illustrated by the model shown in Fig. 5a.

All the sites that displayed this behavior are located along two parallel GBs separating a sub-grain, a configuration typical of coherent twins. Even in the absence of inhibitors, CTs have been reported to have no preferential reactivity compared to adjacent grains, both in acidic[22,25] and alkaline[24,26] media. Thus, since there is passivation in the absence of the inhibitor as confirmed above, the absence of preferential local reactivity in these sites can be assigned to the pre-formed organic film of inhibitor equally blocking surface oxide formation and thus passivation in the GB region and on the adjacent grains, but also equally mitigating the residual reactivity, anodic dissolution or passivation, that may occur in the Cu(I) potential range. This absence of preferential GB reactivity for coherent twins, also observed in acid medium in the presence of inhibitor,[65,66] is interpreted as an intrinsic property of CTs rather than as an inhibiting effect of MBT or MBI.

Intergranular passivation blocked with residual preferential dissolution at GBs.—The local GB sites that showed preferential reactivity compared to adjacent grains characterized by an increase of the depth of the GB surface region upon anodic polarization and after subsequent reduction are labeled from 5 to 25 in Fig. 3a and from 5 to 23 in Fig. 3b for MBT and MBI, respectively. The corresponding histograms of the measured GB depth values are presented in Figure S3a and b in Supplementary Information, respectively. The model in Fig. 5b can help us understand this case of a continuous increase of the GB depth assigned to residual intergranular dissolution.

As discussed above, in our testing conditions, when the cathodic pretreatment is applied to the surface to reduce the native oxide, there is already an organic layer pre-adsorbed on the surface. Upon reductive decomposition of the native oxide, Cu atoms are released and most likely trapped in the inhibitor surface film. The reversible part of the residual electrochemical activity measured during subsequent cycling corresponds to these Cu atoms trapped in the surface organic film and reacting reversibly during the anodic and cathodic sweeps. Along with the copper reacting reversibly, some copper is lost due to dissolution, which forms the irreversible part of the measured electrochemical activity. This residual dissolution in the presence of an inhibitor layer occurs preferentially from intergranular regions resulting in a continuous increase of the depth of the measured line profile. Thus, in the GB sites showing this behavior, the pre-formed inhibitor layers of MBT or MBI block oxide formation in the Cu(I) oxidation range, like on the grains. Still, they fail to completely block residual anodic dissolution in the most reactive sites, resulting in an increase of the depth of the intergranular regions. The GB depth further increases when the surface is measured in the reduced state since, during the reverse scan, there is still polarization in the Cu(I) anodic region before entering the cathodic region.

For MBT, eighteen of the twenty-one sites in Fig. 3a showing this type of behavior belong to the class of random boundaries (sites 5, 6, 8–20 and 23–25). The histogram (Figure S3a) shows that the highest increase in the GB depth, and thus the largest extent of

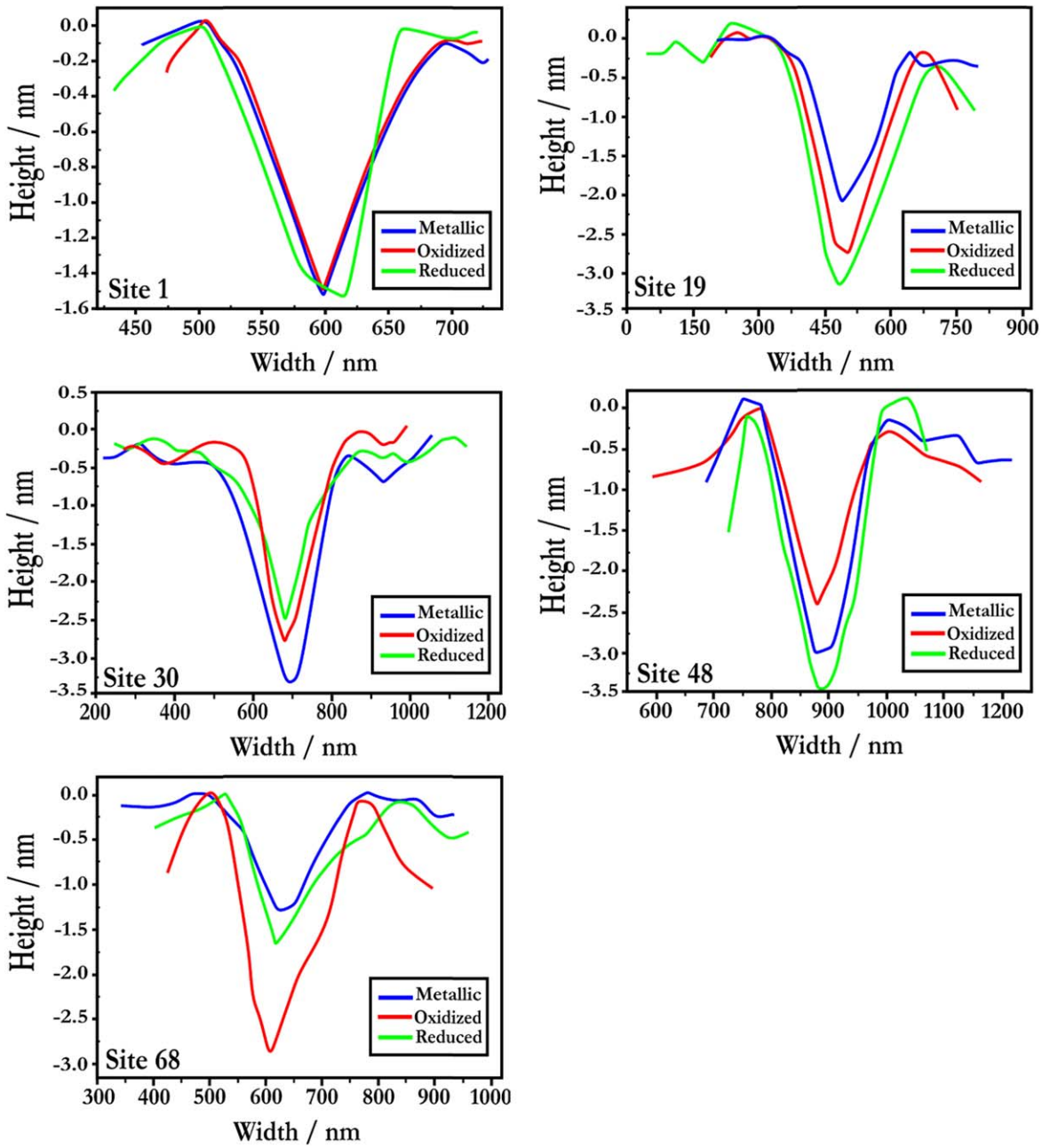

Figure 4. Local evolution behavior of the GB network from average topographic line profiles measured across the GBs for sites indexed in figure 3a. Site #1: no variation of the GB depth; site #19: repeated increase of the GB depth; site #30: repeated decrease of the GB depth; site #48: decrease followed by increase of the GB depth; site #68: increase followed by decrease of the GB depth.

residual dissolution, is measured for this class of grain boundaries. Among the three non-random boundaries, site 7 belongs to the class of CTs. Unlike sites 1–4, also assigned to CTs, this site would not resist residual anodic dissolution, possibly as a result from a significant deviation from the ideal geometry of CTs.[25,26] Sites 21 and 22 belong to the classes of low Σ and high Σ CSL boundaries, respectively. For these three non-random boundaries, it can be observed that the pre-formed MBT layer mitigates the local loss of Cu from the intergranular region to a greater extent than for the other eighteen random GBs, in agreement with the expected more reactive character of random boundaries.

For MBI, we found nineteen sites showing this type of behavior. Eight of them, sites 6, 11, 12, 14–18, belong to the class of random boundaries, and another eight of them, sites 5, 7, 13, 19–23, to the class of high Σ CSL GBs. Three GBs, at sites 8–10, belong to the class of CTs that probably deviate locally from the ideal geometry.

Intergranular passivation incompletely blocked with residual formation of non-reducible passivation products at GBs.—Third is the case of the intergranular behavior characterized by a decrease of the measured GB depth upon anodic polarization in the Cu(I) passive range and after subsequent reduction. For MBT, there were nine sites, labeled 26–34 in Fig. 3a, showing this behavior, and for MBI, twenty-nine sites, labeled 24–52 in Fig. 3b. The corresponding histograms of the measured GB depth are displayed in Figure S4a and b in Supplementary Information, respectively. The model in Fig. 5c illustrates our interpretation of this locally observed intergranular behavior.

In the GB sites showing this type of behavior, copper is preferentially consumed upon anodic polarization compared to adjacent grains to form products that accumulate in the intergranular region, thus leading to the measured decrease of the depth of the GB region. The decrease of the measured GB depth can result from local

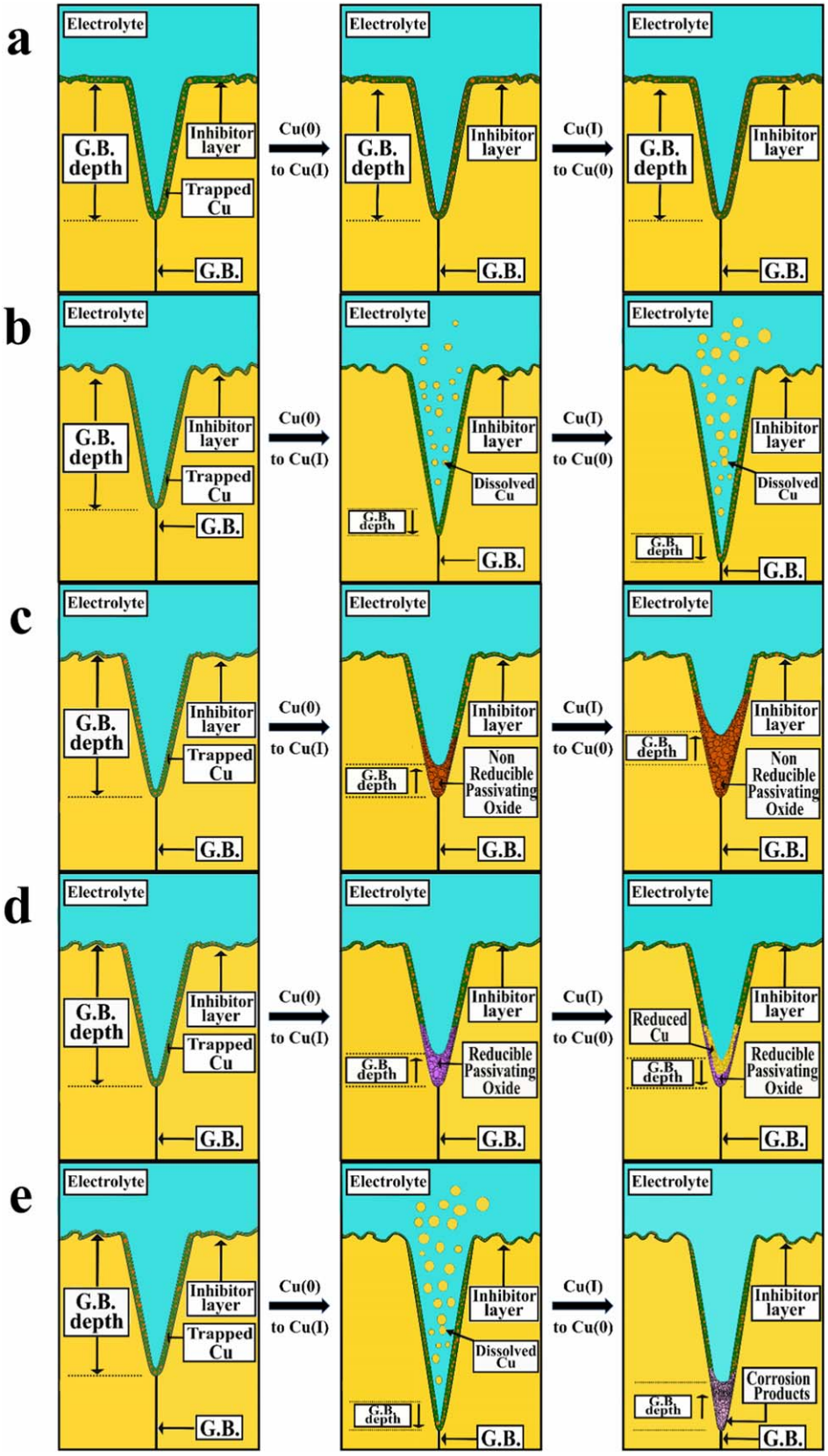

Figure 5. Schematic illustration of observed effects of pre-formed MBT and MBI layers on intergranular passivation: (a) surface passivation is equally blocked on grains and at GB; there is no preferential residual reactivity at the GB; (b) passivation is equally blocked on grains and at GB; there is residual preferential dissolution at the GB; (c) passivation is blocked on grains but incompletely at GB; there is residual anodic reactivity at the GB leading to local formation of non-reducible passivating oxide; (d) passivation is blocked on grains but incompletely at GB; there is residual anodic reactivity at the GB leading to local formation of reducible passivating oxide; (e) passivation is equally blocked on grains and at GB; there is residual dissolution at the GB leading to local accumulation of corrosion products.

passivation during the anodic scan to form Cu(I) oxide like observed in the absence of inhibitor.[23,24,26] This implies that anodic passivation would be incompletely blocked by a pre-formed organic layer, more defective in the GB site than on the adjacent grains, and that Cu(I) oxide would grow where the organic film defectively blocks surface oxidation. Local accumulation of corrosion products cannot be ruled out. They might be complexes formed by the reaction of locally dissolving copper with the organic molecules present in the electrolyte and deposited in the intergranular regions. It is a limitation of the ECSTM analysis as we cannot identify the exact

nature and composition of these accumulated passivation/corrosion products. One could expect Cu(I) oxide to be reduced during the cathodic sweep thus leading to an increase of the GB depth and not the observed decrease[23,24,26] in the final reduced state. However, it is unclear if the applied cathodic sweep would be sufficiently reductive to decompose the Cu(I) oxide formed in the GB sites because of the effect of the pre-formed inhibitor layer.

For MBT, among the nine sites showing this intergranular behavior, one, site 28 is classified as a CT that, just like the above discussed site 7, might be a boundary largely deviated from the ideal geometry of CTs and thus losing its intrinsically intergranular resistant character. Sites 33 and 26 are attributed to low Σ and high Σ CSL boundaries, respectively. Six out of the nine sites are classified as random boundaries with, among them, four sites (sites 27, 29, 30 and 34) showing the largest variation of the GB depth. This preferential intergranular residual activity is expected for random boundaries that are more reactive than CTs and most CSL boundaries. It is here observed even in the presence of corrosion inhibitor.

For MBI, among the twenty-nine sites showing this intergranular behavior, a majority of fifteen (sites 25, 26, 29, 30, 32–38, 44, 45, 51 and 52) is classified as random boundaries with preferential intergranular residual passivation not fully blocked by the pre-formed organic inhibitor layer. Site 43 is classified as a Σ3 CT, likely also deviated from ideal geometry. Sites 27 and 28 are classified as low Σ CSLs, and eleven sites (24, 31, 39–42, 46–50) belongs to the high Σ CSLs.

Intergranular passivation incompletely blocked with residual formation of reducible passivation products at GBs.—Next, the case of the intergranular behavior characterized by a decrease of the GB depth measured upon anodic polarization in the Cu(I) passive range followed by an increase after subsequent reduction is discussed (Figure S5a and b in Supplementary Information). For MBT, there are fourteen sites, labeled 35–48 in Fig. 3a where this behavior is observed, and, for MBI, twenty-six sites, labeled 53–78 in Fig. 3b. This behavior can be understood using the model shown in Fig. 5d.

Like in the previous case, the decrease of the depth measured in the GB surface regions is interpreted as due to the formation of Cu (I) passivation products in the intergranular region when the surface is anodically polarized in the Cu(I) passive region, as a result of a locally less poisoning effect of the pre-formed MBT or MBI layer on formation of Cu(I) oxide. Subsequently, when the surface is cathodically polarized, the increase of the GB depth might be due to electrochemical reduction of the Cu(I) passivation products causing a decrease of thickness. In this case, the applied cathodic sweep would be sufficiently reductive to decompose the Cu(I) oxide products formed in the GB sites. The residual dissolution of copper from the grain boundary region during the cathodic sweep cannot be excluded since there is still polarization in the Cu(I) anodic region before entering the cathodic region. This is suggested by the minority number of GB sites (sites 37–41, 44, 47 and 48 in Figure S5a and sites 53, 54, 60, 64 and 78 in Figure S5b) where the depth is measured larger after anodic/cathodic cycling than before.

For MBT, among the fourteen sites showing this local behavior, ten (sites 38–44 and 46–48) are classified as random boundaries. Site 36 is classified as being a CT, likely deviated from its ideal geometry. Two sites, 37 and 45, are classified as being low Σ CSLs, and one (site 35) as being a high Σ CSL. For MBI, out of twenty-six sites with this behavior, twelve (sites 53, 54, 56, 60–62, 66, 74, 75 and 77) are random boundaries, fourteen (sites 57–59¸ 63–65, 67–73, 76) are high Σ CSLs and two (sites 55 and 78) are attributed to CTs. None of the measured sites are attributed to low Σ CSLs.

Intergranular passivation blocked with residual preferential dissolution and accumulation of corrosion products at GBs.—Finally, we consider the case of the intergranular behavior characterized by an increase of the GB depth measured upon anodic polarization in the Cu(I) passive range followed by a decrease after subsequent reduction. For MBT, this behavior is observed in fifty-two sites labeled 49–101 in Fig. 3a. For MBI, there are twenty-two grain sites, labeled 79–100 in Fig. 3b, having this behavior. The corresponding histograms are shown in Figure S6a and b, respectively. Our interpretation of this behavior is illustrated in Fig. 5e.

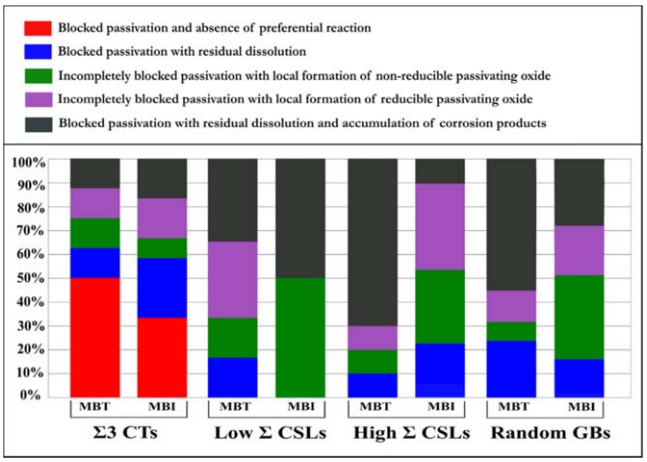

Figure 6. Percentage of each type of intergranular behavior observed on various types of grain boundaries for microcrystalline copper in 0.1 M NaOH (aq) + 1 mM MBI and in 0.1 M NaOH(aq) + 1 mM MBT.

Like in the second case examined, the increase of the depth of the GB surface regions measured upon polarization in the Cu(I) potential range is interpreted as due to the pre-formed organic layer blocking passivation in the GB region but failing to suppress anodic dissolution. Subsequently, during the cathodic sweep, there is ongoing dissolution since there is still polarization in the Cu(I) anodic region before entering the cathodic region, leading in this case to the accumulation of corrosion products in the GB region that might be redeposited Cu-MBT(I) complexes.

For MBT, among the fifty-two sites showing this behavior, forty-two (sites 49, 51, 55–57, 59–77, 81–84, 87–94, 96–99) correspond to random GBs, seven (sites 50, 52–54, 58, 78, 79) belong to high Σ CSL boundaries, two (sites 80, 100) to low Σ CSLs, and one (site 95) to CTs. It has to be noted that data from more sites could be extracted for the experiment with MBT, all of them showed this behavior and correspond to random boundaries. For MBI, twenty-two sites show this local behavior. Among them, fourteen (sites 79, 80, 83 and 85–95) are classified as random boundaries. Two sites (97 and 98) belong to Σ3 CTs, also likely deviated from ideal geometry. Two sites (96 and 99) are attributed to low Σ CSLs and four sites (81, 82, 84 and 100) to high Σ CSLs.

MBT & MBI effects on local passivation properties according to GB type.—Table II summarizes the occurrences of the five types of intergranular behavior observed upon anodic passivation and subsequent reduction in the tested conditions. They are sorted according to GB type as defined in Table I. Figure 6 presents an overall comparative view of the data. Both inhibitors were observed to block surface oxide formation and thus passivation on the grains with residual intergranular dissolution or oxide formation, depending on the local effect of the pre-formed MBT or MBI surface layers and on the GB type.

Coherent twin is the only GB type for which passivation by surface oxide growth was blocked as on the adjacent grains and no residual intergranular activity was detected. With both inhibitors, this was observed for a majority, absolute or relative, of the analyzed sites, which we assign to CTs close to ideal geometry 25, and thus intrinsically resistant to preferential dissolution or preferential oxide growth. In the CT sites deviated from the ideal geometry and thus showing preferential reactivity compared to adjacent grains, all other

Table II. Observed occurrences of intergranular behavior types for various types of grain boundaries for microcrystalline copper in 0.1 M NaOH(aq) + 1 mM of MBT or MBI.

Intergranular behavior	Inhibitor	CTs	Low Σ CSLs	High Σ CSLs	Random GBs
	MBT	4	—	—	—
Blocked passivation and absence of preferential reaction	MBI	4	—	—	—
	MBT	1	1	1	19
Blocked passivation with residual dissolution	MBI	3	—	8	8
	MBT	1	1	1	6
Incompletely blocked passivation with local formation of non-reducible passivating oxide	MBI	1	2	11	15
	MBT	1	2	1	10
Incompletely blocked passivation with local formation of reducible passivating oxide	MBI	2	–	14	10
	MBT	1	2	7	42
Blocked passivation with residual dissolution and accumulation of corrosion products	MBI	2	2	4	14

types of intergranular behavior were observed with a rather uniform distribution of their occurrences. A larger proportion of reactive CT sites were observed with the pre-formed MBI layer than with the pre-formed MBT layer, but this may be due to the site distribution in the analyzed field of view and not to a lower inhibiting efficiency of MBI.

The intergranular behaviors observed for all other types of GBs, low Σ CSLs, high Σ CSLs and random GBs, in the presence of the inhibitors belong to two classes depending on the local poisoning effect of the pre-formed organic layer on the formation of the passivating Cu(I) surface oxide. If intergranular passivation is blocked, residual reactivity is associated to dissolution with possible accumulation of corrosion products. This is color-coded in green and purple in Fig. 6. Whereas, if intergranular passivation is incompletely blocked, Cu(I) oxide products (reducible or not) may form in the intergranular region. This is coded in blue and black in Fig. 6.

Examining the data for random GBs in Fig. 6 from this perspective, we can deduce a stronger barrier effect on intergranular passivation of MBT than of MBI. Random boundaries can be expected to be the most reactive owing to their defective crystallographic character. With MBI, the residual formation of passivating oxide products, whether reducible or not, for most of the random boundaries, is in agreement with previous studies showing that, due to higher reactivity of these GBs, a locally thicker film of Cu(I) oxide film is formed in the absence of inhibitor 22,23,25. With MBT, intergranular passivation would be more strongly poisoned by the pre-formed organic layer than with MBI and thus the residual formation of passivating Cu(I) oxide products less frequently occurring in the analyzed distribution.

For high Σ CSLs, Fig. 6 also shows that MBT would more strongly poison passivation than MBI, thus confirming for these reactive boundaries the trend observed for random GBs. For low Σ CSLs, the distribution that could be analyzed in the field of view is smaller. However, Fig. 6 shows that the barrier effects of both inhibitors on intergranular passivation, fully blocking or not surface oxide growth, are much more balanced. In these GBs, the residual reactivity would be too low to differentiate the barrier effect on the passivation behavior, which is in line with the less reactive character of the low Σ CSLs that can be expected from their ordered crystallographic character.

The stronger barrier effect of MBT than MBI for blocking intergranular passivation is likely to result from the properties of the pre-formed organic inhibitor layer. As discussed from the analysis of the global electrochemical data, more Cu atoms would be trapped in the pre-formed MBT than in the pre-formed MBI surface layer after reductive decomposition of the native oxide in the presence of the inhibitor. This increase in trapped Cu atoms could reflect an increase in thickness and/or a densification of the MBT surface layer compared to the MBI surface layer, which would improve the barrier properties against passivation by surface oxide growth, especially in the more reactive sites such as intergranular boundaries. This enhanced barrier properties could result from the presence in the heterocyclic structure of two S and one N atom in MBT versus one S and two N atoms in MBI, with S atoms being able to covalently bond more strongly to Cu atoms than N atoms.

Conclusions

ECSTM was applied to characterize the effects of MBT and MBI on the local passivation and corrosion properties at the surface termination of grain boundaries for copper in alkaline aqueous solution. The macroscopic electrochemical response, characterized by CV, showed that, in the presence of 1 mM of inhibitor, both MBT and MBI block surface oxide growth and thus passivation on the grains. The observed residual activity was attributed to reversible anodic oxidation of copper atoms that were dissociated from the native oxide and trapped in the pre-formed organic film and to irreversible loss of copper due to residual dissolution in the most reactive sites, including GBs.

In situ ECSTM analysis of the same GB sites in the initial Cu(0) metallic, Cu(I) oxidized and Cu(0) reduced surface states showed that coherent twins with close to ideal geometry did not react preferentially compared to the adjacent grains in agreement with previous reports. All the other types of GBs, including CTs deviated from ideal geometry, i.e. incoherent twins, were preferential sites of reaction compared to grains. Depending on the barrier effect of the pre-formed organic surface layer, intergranular passivation by surface oxide growth was found to be either completely blocked, however with residual local dissolution and accumulation of corrosion products in the GBs regions, or incompletely blocked, with residual local formation of passivating oxide, likely Cu(I) oxides.

For the less reactive GBs corresponding to low Σ CSLs, no difference of barrier effect of the pre-formed MBT and MBI organic layers for fully blocking passivation or not was observed. For the more reactive GBs corresponding to random boundaries and high Σ CSLs, the pre-formed MBT surface layer showed a stronger barrier effect for blocking surface oxide formation than the pre-formed MBI surface layer as shown by the higher occurrence of blocked intergranular passivation in the analyzed population of GB sites. It is proposed that MBT, being able to strongly bond to more Cu atoms than MBI thanks to two S atoms instead of one in its heterocyclic structure, would more efficiently trap Cu atoms from the surface, thus providing improved barrier properties to the pre-formed MBT surface layer, including in the most reactive surface sites such as GBs.

Acknowledgments

This project has received funding from the European Research Council (ERC) under the European Union's Horizon 2020 research and innovation programme (ERC Advanced Grant agreement No 741123).

ORCID

Sagar B. Sharma https://orcid.org/0000-0001-8118-7580
Vincent Maurice https://orcid.org/0000-0001-5222-9972
Philippe Marcus https://orcid.org/0000-0002-9140-0047

References

1. J. Mieluch and M. Smialowski, "The behaviour of grain boundaries in iron during anodic polarization in ammonium nitrate solution." *Corros. Sci.*, **4**, 237 (1964).
2. P. Lin, G. Palumbo, U. Erb, and K. T. Aust, "Influence of grain boundary character distribution on sensitization and intergranular corrosion of alloy 600." *Scr. Metall. Mater.*, **33**, 1387 (1995).
3. A. Vinogradov, T. Mimaki, S. Hashimoto, and R. Valiev, "On the corrosion behavior of ultra-fine grain copper." *Scr. Mater.*, **41**, 3 (1999).
4. L. Lu, M. L. Sui, and K. Lu, "Superplastic extensibility of nanocrystalline copper at room temperature | science." *Science*, **287**, 1463 (2000).
5. V. Y. Gerrtsman and S. M. Gruemer, "Grain boundary character along intergranular stress corrosion crack paths in austenitic stainless alloys removed from high-temperature water." *Acta Mater.*, **49**, 1589 (2001).
6. S. H. Kim, U. Erb, and K. T. Aust, "Grain boundary character distribution and intergranular corrosion behavior in high purity aluminum." *Scr. Mater.*, **44**, 835 (2001).
7. H. Miyamoto, K. Yoshimura, T. Mimaki, and M. Yamashita, "Behavior of intergranular corrosion of ⟨011⟩ tilt grain boundaries of pure copper bicrystals." *Corros. Sci.*, **44**, 1835 (2002).
8. M. Shimada, H. Kokawa, Z. J. Wang, Y. S. Sato, and I. Karibe, "Optimization of grain boundary character distribution for intergranular corrosion resistant 304 stainless steel by twin-induced grain boundary engineering." *Acta Mater.*, **50**, 2331 (2002).
9. E. M. Lehockey, A. M. Brennenstuhl, and I. Thompson, "On the relationship between grain boundary connectivity, coincident site lattice boundaries, and intergranular stress corrosion cracking." *Corros. Sci.*, **10**, 2383 (2004).
10. V. Randle, "Special' boundaries and grain boundary plane engineering." *Scr. Mater.*, **54**, 1011 (2006).
11. S. Xia, B. Zhou, and W. Chen, "Effect of single-step strain and annealing on grain boundary character distribution and intergranular corrosion in Alloy 690." *J. Mater. Sci.*, **43**, 2990 (2008).

12. R. Jones and V. Randle, "Sensitisation behaviour of grain boundary engineered austenitic stainless steel." *Materials Science and Engineering*, **527**, 4275 (2010).
13. K. D. Ralston and N. Birbilis, "Effect of grain size on corrosion: a review." *Corrosion*, **66**, 075005 (2010).
14. C. L. Changliang, S. Xi, H. Li, T. G. Liu, B. X. Zhou, W. J. Chen, and N. Wang, "Improving the intergranular corrosion resistance of 304 stainless steel by grain boundary network control." *Corros. Sci*, **53**, 1880 (2011).
15. C. Luo, X. Zhou, G. E. Thompson, and A. E. Hughes, "Observations of intergranular corrosion in AA2024-T351: The influence of grain stored energy." *Corros. Sci.*, **61**, 35 (2012).
16. B. Sunil Kumar, B. S. Prasad, V. Kain, and J. Reddy, "Methods for making alloy 600 resistant to sensitization and intergranular corrosion." *Corros. Sci.*, **70**, 55 (2013).
17. Y. Takehara, H. Fujiwara, and H. Miyamoto, "Special' to 'general' transition of intergranular corrosion in Sigma 3{111} grain boundary with gradually changed misorientation." *Corros. Sci.*, **77**, 171 (2013).
18. A. Stratulat, J. A. Duff, T. J. Marrow, and T. James, "Grain boundary structure and intergranular stress corrosion crack initiation in high temperature water of a thermally sensitised austenitic stainless steel, observed in situ." *Corros. Sci.*, **85**, 428 (2014).
19. B. V. Mahesh and R. K. S. Raman, "Role of Nanostructure in Electrochemical Corrosion and High Temperature Oxidation: A Review." *Metall. Mater. Trans. A*, **45**, 5799 (2014).
20. N. Srinivasan, V. Kain, N. Birbilis, K. V. Mani Krishna, S. Shekhawat, and I. Samajdar, "Near boundary gradient zone and sensitization control in austenitic stainless steel." *Corros. Sci.*, **100**, 544 (2015).
21. F. M. A. Kharafi, N. A. Al-Awadi, I. M. Ghayad, R. M. Abdullah, and M. R. Ibrahim, "Novel technique for the application of azole corrosion inhibitors on copper surface." *Mater. Trans.*, **51**, 1671 (2010).
22. E. Martinez-Lombardia, L. Lapeire, V. Maurice, I. De Graeve, K. Verbeken, L. H. Klein, L. Kestens, P. Marcus, and H. Terryn, "In situ scanning tunneling microscopy study of the intergranular corrosion of copper." *Electrochem. Commun.*, **41**, 1 (2014).
23. H. Chen, V. Maurice, L. H. Klein, L. Lapeire, K. Verbeken, H. Terryn, and P. Marcus, "Grain boundary passivation studied by in situ scanning tunneling microscopy on microcrystalline copper." *J. Solid State Electrochem.*, **19**, 3501 (2015).
24. H. Chen, M. Bettayeb, V. Maurice, L. H. Klein, L. Lapeire, K. Verbeken, H. Terryn, and P. Marcus, "Local passivation of metals at grain boundaries: In situ scanning tunneling microscopy study on copper." *Corros. Sci.*, **111**, 659 (2016).
25. M. Bettayeb, V. Maurice, L. H. Klein, L. Lapeire, K. Verbeken, and P. Marcus, "Nanoscale intergranular corrosion and relation with grain boundary character as studied in situ on copper." *J. Electrochem. Soc.*, **165**, 835 (2018).
26. M. Bettayeb, V. Maurice, L. H. Klein, L. Lapeire, K. Verbeken, and P. Marcus, "Combined in situ microstructural study of the relationships between local grain boundary structure and passivation on microcrystalline copper." *Electrochim. Acta*, **305**, 240 (2019).
27. T. Shahrabi, H. Tavakholi, and M. G. Hosseini, "Corrosion inhibition of copper in sulphuric acid by some nitrogen heterocyclic compounds." *Anti-Corrosion Methods and Materials*, **54**, 308 (2007).
28. M. M. Antonijevic and M. B. Petrovic, "Review copper corrosion inhibitors. a review." *Int. J. Electrochem. Sci.*, **3**, 1 (2008).
29. M. M. Antonijević, S. M. Milić, and M. B. Petrović, "Films formed on copper surface in chloride media in the presence of azoles." *Corros. Sci.*, **51**, 1228 (2009).
30. G. Gece, "Drugs: A review of promising corrosion inhibitors." *Corros. Sci.*, **53**, 3873 (2011).
31. P. M. Niamien, F. K. Essy, A. Trokourey, A. Yapi, H. K. Aka, and D. Diabate, "Correlation between the molecular structure and the inhibiting effect of some benzimidazole derivatives." *Mater. Chem. Phys.*, **136**, 59 (2012).
32. M. Petrovic Mihajlovic and M. Antonijevic, "Copper corrosion inhibitors. period 2008-2014. a review." *Int. J. Electrochem. Sci.*, **10**, 1027 (2015).
33. I. Milošev, N. Kovačević, J. Kovač, and A. Kokalj, "The roles of mercapto, benzene and methyl groups in the corrosion inhibition of imidazoles on copper: I. Experimental characterization." *Corros. Sci.*, **98**, 107 (2015).
34. N. Kovačević, I. Milošev, and A. Kokalj, "The roles of mercapto, benzene, and methyl groups in the corrosion inhibition of imidazoles on copper: II. Inhibitor–copper bonding." *Corros. Sci.*, **98**, 457 (2015).
35. A. Fateh, M. Aliofkhazraei, and A. R. Rezvanian, "Review of corrosive environments for copper and its corrosion inhibitors." *Arabian J. Chem.*, **13**, 481 (2020).
36. D. Chadwick and T. Hashemi, "Electron spectroscopy of corrosion inhibitors: Surface films formed by 2-mercaptobenzothiazole and 2-mercaptobenzimidazole on copper." *Surf. Sci.*, **89**, 649 (1979).
37. M. Ohsawa and W. Suëtaka, "Spectro-electrochemical studies of the corrosion inhibition of copper by mercaptobenzothiazole." *Corros. Sci.*, **19**, 709 (1979).
38. T. Yoshida, "An X-ray Photoelectron Spectroscopic Study of Several Metal Complexes of 2-Mercaptobenzimidazole and 2-Mercaptobenzoxazole." *BCSJ*, **53**, 1449 (1980).
39. G. Xue, X.-Y. Huang, J. Dong, and J. Zhang, "The formation of an effective anti-corrosion film on copper surfaces from 2-mercaptobenzimidazole solution." *J. Electroanal. Chem. Interfacial Electrochem.*, **310**, 139 (1991).
40. G. Xue, X. Huang, and J. Ding, "Surface reaction of 2-mercaptobenzimidazole on metals and its application in adhesion promotion." *J. Chem. Soc. Faraday Trans.*, **87**, 1229 (1991).
41. G. Xue and Q. Dai, "SERS and IR Studies of the Reaction of an Oxidized Surface and an Etched Surface of Copper with 2-Mercaptobenzimidazole." *Spectrosc. Lett.*, **27**, 341 (1994).
42. J. C. Marconato, L. O. Bulhões, and M. L. Temperini, "A spectroelectrochemical study of the inhibition of the electrode process on copper by 2-mercaptobenzothiazole in ethanolic solutions." *Electrochim. Acta*, **43**, 771 (1998).
43. F. X. Perrin and J. Pagetti, "Characterization and mechanism of direct film formation on a cu electrode through electro-oxidation of 2-mercaptobenzimidazole." *Corros. Sci.*, **40**, 1647 (1998).
44. C. W. Yan, H. C. Lin, and C. N. Cao, "Investigation of inhibition of 2-mercaptobenzoxazole for copper corrosion." *Electrochim. Acta*, **45**, 2815 (2000).
45. R. Woods, G. A. Hope, and K. Watling, "A SERS spectroelectrochemical investigation of the interaction of 2-mercaptobenzothiazole with copper, silver and gold surfaces." *J. Appl. Electrochem.*, **30**, 1209 (2000).
46. B. Trachli, M. Keddam, H. Takenouti, and A. Srhiri, "Protective effect of electropolymerized 2-mercaptobenzimidazole upon copper corrosion." *Progress in Organic Coatings*, **44**, 17 (2002).
47. D.-Q. Zhang, L.-X. Gao, and G. Zhou, "Inhibition of copper corrosion in aerated hydrochloric acid solution by heterocyclic compounds containing a mercapto group." *Corrosion Science - CORROS SCI*, **46**, 3031 (2004).
48. L. P. Kazansky, I. A. Selyaninov, and Y. I. Kuznetsov, "Adsorption of 2-mercaptobenzothiazole on copper surface from phosphate solutions." *Appl. Surf. Sci.*, **258**, 6807 (2012).
49. J. Izquierdo, J. J. Santana, S. González, and R. M. Souto, "Scanning microelectrochemical characterization of the anti-corrosion performance of inhibitor films formed by 2-mercaptobenzimidazole on copper." *Prog. Org. Coat.*, **74**, 526 (2012).
50. M. Finšgar, "2-Mercaptobenzimidazole as a copper corrosion inhibitor: Part I. Long-term immersion, 3D-profilometry, and electrochemistry." *Corros. Sci.*, **72**, 82 (2013).
51. M. Finšgar, "2-Mercaptobenzimidazole as a copper corrosion inhibitor: Part II. Surface analysis using X-ray photoelectron spectroscopy." *Corros. Sci.*, **72**, 90 (2013).
52. M. Finšgar and D. Kek Merl, "An electrochemical, long-term immersion, and XPS study of 2-mercaptobenzothiazole as a copper corrosion inhibitor in chloride solution." *Corros. Sci.*, **83**, 164 (2014).
53. G. Žerjav and I. Milošev, "Protection of copper against corrosion in simulated urban rain by the combined action of benzotriazole, 2-mercaptobenzimidazole and stearic acid." *Corros. Sci.*, **98**, 180 (2015).
54. Y.-H. Chen and A. Erbe, "The multiple roles of an organic corrosion inhibitor on copper investigated by a combination of electrochemistry-coupled optical in situ spectroscopies." *Corros. Sci.*, **145**, 232 (2018).
55. Z. Zhang, Q. Wang, X. Wang, and L. Gao, "The influence of crystal faces on corrosion behavior of copper surface: First-principle and experiment study." *Appl. Surf. Sci.*, **396**, 746 (2017).
56. X. Wu, F. Wiame, V. Maurice, and P. Marcus, "Adsorption and thermal stability of 2-mercaptobenzothiazole corrosion inhibitor on metallic and pre-oxidized Cu(111) model surfaces." *Appl. Surf. Sci.*, **508**, 145132 (2020).
57. X. Wu and F. Wiame, V. Maurice and P. Marcus, "2-Mercaptobenzothiazole corrosion inhibitor deposited at ultra-low pressure on model copper surfaces." *Corros. Sci.*, **166**, 108464 (2020).
58. X. Wu, F. Wiame, V. Maurice, and P. Marcus, "2-Mercaptobenzimidazole films formed at ultra-low pressure on copper: adsorption, thermal stability and corrosion inhibition performance." *Appl. Surf. Sci.*, **527**, 146814 (2020).
59. X. Wu, F. Wiame, V. Maurice, and P. Marcus, "Moiré Structure of the 2-Mercaptobenzothiazole Corrosion Inhibitor Adsorbed on a (111)-Oriented Copper Surface." *J. Phys. Chem. C*, **124**, 15995 (2020).
60. E. Vernack, D. Costa, P. Tingaut, and P. Marcus, "DFT studies of 2-mercaptobenzothiazole and 2-mercaptobenzimidazole as corrosion inhibitors for copper." *Corros. Sci.*, **174**, 108840 (2020).
61. F. Chiter, D. Costa, V. Maurice, and P. Marcus, ", "Adsorption of 2-mercaptobenzimidazole corrosion inhibitor on copper: DFT study on model oxidized interfaces." *J. Electrochem. Soc.*, **167**, 161506 (2020).
62. F. Chiter, D. Costa, V. Maurice, and P. Marcus, "DFT investigation of 2-mercaptobenzothiazole adsorption on model oxidized copper surfaces and relationship with corrosion inhibition." *Appl. Surf. Sci.*, **537**, 147802 (2021).
63. X. Wu, F. Wiame, V. Maurice, and P. Marcus, "2-mercaptobenzimidazole films formed at ultra-low pressure on copper: adsorption, thermal stability and corrosion inhibition performance." *Appl. Surf. Sci.*, **527**, 146814 (2020).
64. X. Wu, F. Wiame, V. Maurice, and P. Marcus, *"Molecular scale insights into interaction mechanisms between organic inhibitor film and copper", npj Materials Degradation*, **5**, 22 (2021).
65. S. B. Sharma, V. Maurice, L. H. Klein, and P. Marcus, "Local Inhibition by 2-mercaptobenzothiazole of early stage intergranular corrosion of copper." *J. Electrochem. Soc.*, **167**, 161504 (2020).
66. S. B. Sharma, V. Maurice, L. H. Klein, and P. Marcus, "Early stage intergranular corrosion of copper and local inhibition effects of 2-mercaptobenzimidazole." *Electrochemica Acta*, **378**, 138150 (2021).
67. H.-H. Strehblow and B. Titze, "The investigation of the passive behaviour of copper in weakly acid and alkaline solutions and the examination of the passive film by esca and ISS." *Electrochim. Acta*, **25**, 839 (1980).
68. U. Sander, H. H. Strehblow, and J. K. Dohrmann, "In situ photoacoustic spectroscopy of thin oxide layers on metal electrodes. Copper in alkaline solution." *J. Phys. Chem.*, **85**, 447 (1981).
69. M. R. G. De Chialvo, R. C. Salvarezza, and A. Arvia, "The mechanism of oxidation of copper in alkaline solutions." *J. Appl. Electrochem.*, **14**, 165 (1984).
70. S. T. Mayer and R. H. Muller, "An In Situ Raman Spectroscopy Study of the Anodic Oxidation of Copper in Alkaline Media." *J. Electrochem. Soc.*, **139**, 426 (1992).

71. C. A. Melendres, G. A. Bowmaker, J. M. Leger, and B. Beden, "In-situ synchrotron far infrared spectroscopy of surface films on a copper electrode in aqueous solutions." *J. Electroanal. Chem.*, **449**, 215 (1998).
72. W. Kautek and J. G. G. Ii, "XPS Studies of anodic surface films on copper electrodes." *J. Electrochem. Soc.*, **137**, 2672 (1990).
73. B. Millet, "Etude électrochimique et photoélectrochimique de couches d'oxydes de cuivre semi-conductrices. Rôle d'un inhibiteur de corrosion du cuivre." *PhD thesis*, Université Paris VI (1994).
74. Y. Feng, K.-S. Siow, W.-K. Teo, K.-L. Tan, and A.-K. Hsieh, "Corrosion Mechanisms and Products of Copper in Aqueous Solutions at Various pH Values." *Corrosion*, **53**, 389 (1997).
75. H. Y. H. Chan, C. G. Takoudis, and M. J. Weaver, "Oxide film formation and oxygen adsorption on copper in aqueous media as probed by surface-enhanced Raman spectroscopy." *J. Phys. Chem. B*, **103**, 357 (1999).
76. V. Maurice, H.-H. Strehblow, and P. Marcus, "In situ STM study of the initial stages of oxidation of Cu(111) in aqueous solution." *Surf. Sci.*, **458**, 185 (2000).
77. J. Kunze, V. Maurice, L. H. Klein, H.-H. Strehblow, and P. Marcus, "In situ scanning tunneling microscopy study of the anodic oxidation of Cu(111) in 0.1 M NaOH." *J. Phys. Chem. B*, **105**, 4263 (2001).
78. H.-H. Strehblow, V. Maurice, and P. Marcus, "Initial and later stages of anodic oxide formation on Cu, chemical aspects, structure and electronic properties." *Electrochim. Acta*, **46**, 3755 (2001).
79. J. Kunze, V. Maurice, L. H. Klein, H.-H. Strehblow, and P. Marcus, "In situ STM study of the anodic oxidation of Cu(001) in 0.1 M NaOH." *J. Electroanal. Chem.*, **554–555**, 113 (2003).
80. J. Kunze, V. Maurice, L. H. Klein, H.-H. Strehblow, and P. Marcus, "In situ STM study of the duplex passive films formed on Cu(111) and Cu(001) in 0.1 M NaOH." *Corros. Sci.*, **46**, 245 (2004).
81. E. Martinez Lombardia, L. Lapeire, I. De Graeve, H. Terryn, and K. Verbeken, "Influence of grain size on the electrochemical behavior of pure copper." *J. Mater. Sci.*, **52**, 1501 (2017).
82. E. Martinez-Lombardia, Y. Gonzalez-Garcia, L. Lapeire, I. De Graeve, K. Verbeken, L. Kestens, J. Mol, and H. Terryn, "Scanning electrochemical microscopy to study the effect of crystallographic orientation on the electrochemical activity of pure copper." *Electrochim. Acta*, **116**, 89 (2014).
83. E. Martinez-Lombardia, V. Maurice, L. Lapeire, I. De Graeve, K. Verbeken, L. H. Klein, L. Kestens, P. Marcus, and H. Terryn, "In situ scanning tunneling microscopy study of grain-dependent corrosion on microcrystalline copper." *J. Phys. Chem. C*, **118**, 25421 (2014).
84. R. Lindström, V. Maurice, and L. H. Klein, *The Use of Electrochemical Scanning Tunnelling Microscopy (EC-STM) in Corrosion Analysis | ScienceDirect* (Woodhead Publishing Limited, Cambridge, England) (2007).
85. *Gwyddion – Free* SPM (AFM, SNOM*/NSOM, STM, MFM …) data analysis software*.